ELSEVIER

Journal of Magnetism and Magnetic Materials 200 (1999) 274–289

Journal of magnetism and magnetic materials

www.elsevier.com/locate/jmmm

Current-perpendicular (CPP) magnetoresistance in magnetic metallic multilayers

J. Bass*, W.P. Pratt Jr.

Department of Physics and Astronomy, Center for Fundamental Materials Research and NSF MRSEC Center for Sensor Materials, Michigan State University, East Lansing, MI 48824-1116, USA

Received 7 January 1999; received in revised form 9 February 1999

Abstract

We present an experimentalist's view of the theory and published data for the magnetoresistance (MR) of a multilayer composed of alternating ferromagnetic (F) and non-magnetic (N) metals measured with current flow perpendicular to the layer planes (CPP-MR). We explain the advantages of this geometry for determining the fundamental quantities underlying spin-polarized transport, describe the different techniques developed to measure the CPP-MR, summarize the salient features of the models used to analyze experimental data, and describe tests of those models. We then review what has been learned so far about spin-dependent scattering anisotropy and spin relaxation in F-metals and at F/N interfaces, specific resistances of F/N interfaces, the temperature dependence of spin-polarized transport parameters, and mixing of the spin-polarized electron currents. After a brief overview of some new directions, we conclude with a list of questions still to be answered.

Keywords: Giant magnetoresistance; Magnetic multilayers; Spin-polarized transport; Magnetoresistance; Metallic multilayers

1. Introduction

The discovery of giant magnetoresistance (GMR) in $[F/N]_N$ multilayers, composed of N bilayers of alternating ferromagnetic (F) and non-magnetic (N) layers [1,2], has led both to new technology [3][1] and to growth of a new field of study, spin-polarized transport [4–7]. The fundamental physics of spin-polarized transport involves: (a) differential rates of scattering (anisotropic scattering), both within F-layers and at F/N interfaces, of electrons with spin along (↑) or opposite to (↓) the local magnetization, $\boldsymbol{M}_i$; (b) rates of loss of spin-direction memory (spin relaxation) within F- and N-layers and at F/N interfaces; and (c) rates of mixing of spin-polarized currents. This review describes what has been learned about these quantities from measurements of the current perpendicular to plane (CPP)-MR. Paraphrasing Ref. [5]: (a) the high symmetry of the CPP-MR makes its theory simpler than that of either the more usual current in plane (CIP)-MR or the MR of granular multilayers; and (b) the CPP-MR is also less sensitive to unavoidable sample inhomogeneities, making it better suited for testing theoretical models

* Corresponding author. Tel.: + 1-517-3432-1146; fax: + 1-517-353-4500.

E-mail address: bass@pa.msu.edu (J. Bass)

[1] E.g., the web-pages of Non-Volatile Electronics and IBM, Almaden.

0304-8853/99/$ - see front matter
PII: S0304-8853(99)00316-9

and elucidating the fundamental physics of spin-polarized transport, including accessing the fundamental parameters. The CPP-MR is also usually larger than the CIP-MR (Figs. 1–3) [8–13], and becomes more competitive as device size shrinks.[2]

In this review we focus on diffusive CPP transport at the Fermi energy and for normal current densities. Ballistic transport, transport away from the Fermi energy, and experiments involving high current density, will only be briefly noted. The review is organized as follows. Section 2 defines the GMR and describes its source in anisotropic scattering. Section 3 defines the CPP spin-polarized transport parameters. Section 4 outlines the different experimental techniques used to measure the CPP-MR and their advantages and disadvantages. Section 5 describes ways to controllably achieve the parallel (P) and anti-parallel (AP) ordering of the $\boldsymbol{M}_i$'s of adjacent F-layers needed for quantitative analysis. The two most flexible of these, hybrid spin valves and exchange-biased spin valves, are becoming increasingly important in CPP-MR studies. Section 6 reviews the models used to analyze CPP-MR data. It starts with the simple two-current series-resistor (2CSR) model and experiments on Co/Cu and Co/Ag multilayers used to test its applicability, and then proceeds to the more complex Valet–Fert (VF) equations [14] for finite spin-diffusion lengths, l_{sf}, that seem often to be needed when the F- or N-layers are alloys. Sections 7–11 describe what has been learned from CPP-MR measurements about the spin polarized-transport parameters. The latest studies mostly involve application of the VF equations to CPP-MR measurements on spin valves. Section 12 describes some new directions for CPP studies, and Section 13 contains a summary and a list of questions still to be answered.

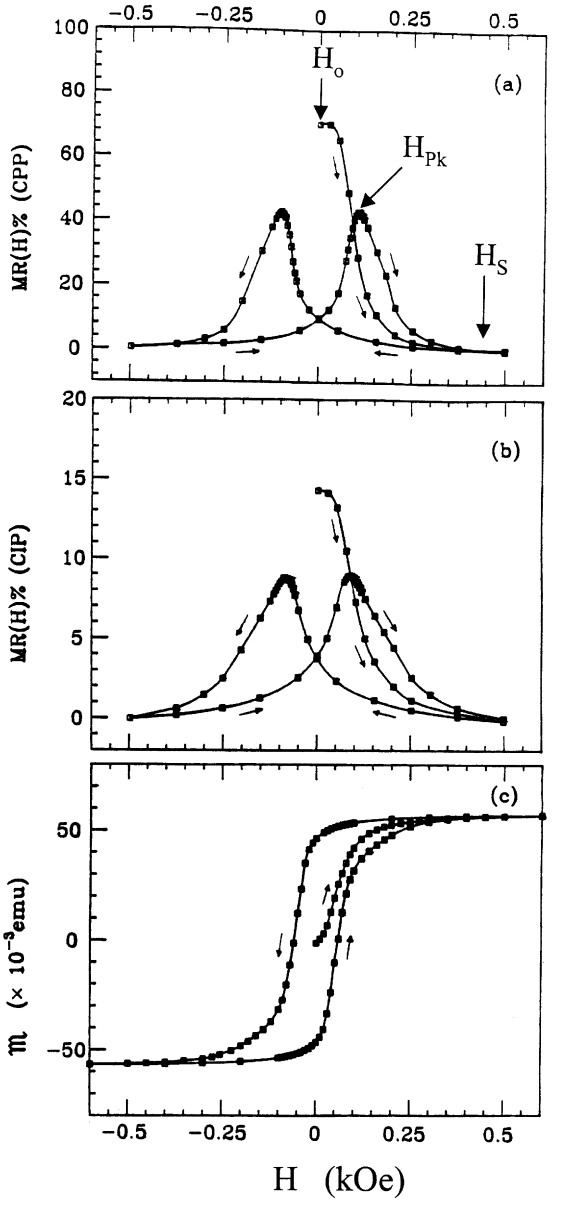

Fig. 1. CPP- and CIP-MRs, and magnetization, M, for a sputtered $[Co(6\ nm)/Ag(6\ nm)]_{60}$ multilayer at 4.2 K. The field of the maximum resistance, in the as-prepared sample, is designated H_0, the saturation field is designated H_s, and the field of the local maximum after saturation is designated H_{Pk}. Note that H_{Pk} is close to the coercive field, H_c. The curves are just guides to the eye (after Ref. [9]).

2. Definition of GMR and the physics underlying it

GMR is an often large change in resistance (usually a decrease) when a strong enough magnetic

[2] The CPP resistance increases with decreasing sample area A, becoming $\sim \Omega$ only at submicron dimensions.

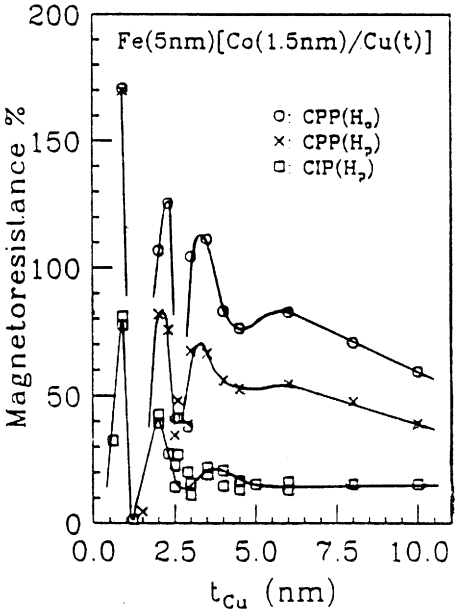

Fig. 2. CIP-MR and CPP-MR for a series of $[Co(1.5\,nm)/Cu(t)]_N$ multilayers. The open squares are the CIP-MR at H(Pk); the crosses the CPP-MR at H(Pk); and the open circles the CPP-MR at H(0). The curves are just guides to the eye (from Ref. [10,11]).

field $\boldsymbol{H}$ aligns the $\boldsymbol{M}_i$ of the F layers parallel (P) to each other [1,2]. The MR is usually defined as [9]

$$\mathrm{MR}\% = 100 \times [R(\mathrm{AP}) - R(\mathrm{P})]/R(\mathrm{P}) = \Delta R/R(\mathrm{P}) \quad (1)$$

where R(P) is the resistance above the F-layer saturation field H_s, and R(AP) the resistance when the $\boldsymbol{M}_i$ of adjacent layers are aligned antiparallel (AP).

Fig. 4 shows the origin of GMR for anisotropic scattering only within the F-layers [1]. Electrons are divided into two channels that propagate independently, spins along (+) or opposite to (−) the external field $+\boldsymbol{H}$. Electrons with spins (↓) are assumed to be scattered more strongly than those with spins (↑) ($\alpha_F = \rho_F^{\downarrow}/\rho_F^{\uparrow} > 1$, where ρ indicates a resistivity). In Fig. 4a, all of the F-layers are identical. In the AP state, both (+) and (−) electrons scatter strongly in alternate F-layers. In the P state, in contrast, (+) electrons scatter weakly in all F-layers, shorting out the sample and giving R(P) < R(AP). Note that exactly the same behavior is found if electrons with spins (↑) are scattered more strongly ($\alpha_F < 1$). Fig. 4b shows, however, that the GMR can be made 'inverse' – R(P) > R(AP) – by combining two different F-layers, one with $\alpha_F > 1$ and the other with $\alpha_F < 1$. The sample is then shorted out in the AP state. Measurements with two different F-layers thus allow determination of whether α_F is >1 or <1. Exactly analogous pictures can be drawn for scattering anisotropy at the interfaces.

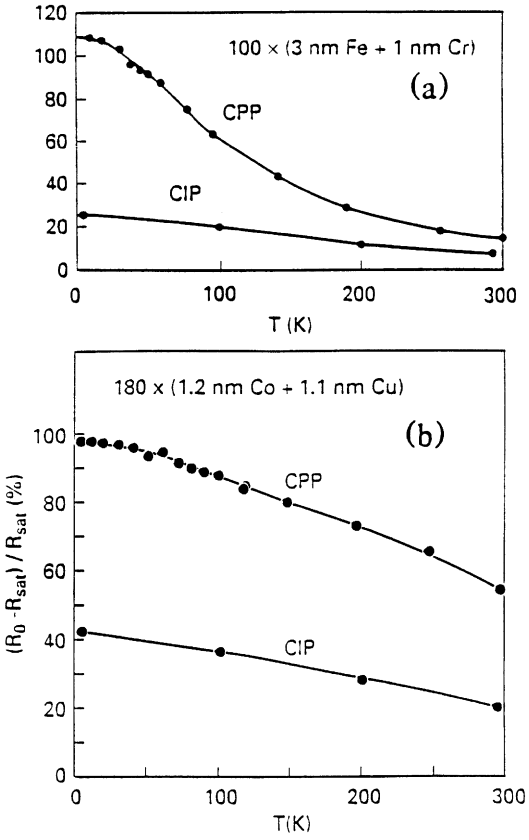

Fig. 3. CPP-MR and CIP-MR versus temperature T for: (a) $[Fe(3\,nm)/Cr(1\,nm)]_{100}$ and (b) $[Co(1.2\,nm)/Cu(1.1\,nm)]_{180}$ multilayers. The curves are just guides to the eye (After, Refs. [12,13]).

3. Spin-polarized transport parameters

In this section we define the parameters used to analyze CPP-MR data. While some parameters are

defined in the same way for the CPP-MR, the CIP-MR, and 'bulk' F-alloys, it is not obvious that they are, in fact, identical. Whether parameters are 'unified' – i.e., can be transferred from one property to another – is a topic just beginning to be addressed [15–19]. Since it is rarely easy to derive reliable parameters for any property, it is important to make such comparisons. As examples of potential benefits, transferability would let decades old values of α_F derived for F-alloys from studies of deviations from Matthiessen's rule [20] be used to predict better alloys for CPP- and CIP-MR devices, and stimulate more theoretical work on the origins of these parameters for F-alloys [21].

3.1. Scattering anisotropy within F-layers and at F/N interfaces

Scattering anisotropy within F-layers is characterized experimentally by the ratio $\alpha_F = (\rho_F^{\downarrow}/\rho_F^{\uparrow})$ already defined [1,20], and scattering anisotropy at F/N interfaces similarly by the equivalent ratio $\alpha_{F/N} = (R_{F/N}^{\downarrow}/R_{F/N}^{\uparrow})$ for the interface resistances. More useful equivalent parameters for the CPP-MR are β and γ given by $\alpha_F = (1+\beta)/(1-\beta)$ and $\alpha_{F/N} = (1+\gamma)/(1-\gamma)$ [14,22]. Section 6 will show that β and γ directly determine the CPP-MR, which is zero when both are zero. A complete set of parameters requires specifying the strengths of the scattering of polarized electrons. For the CPP-MR the most convenient are [14,22] $\rho_F^* = (\rho_F^{\uparrow} + \rho_F^{\downarrow})/4 = \rho_F/(1-\beta^2)$, a renormalized version of the resistivity ρ_F of the F-layer, and $AR_{F/N}^* = AR_{F/N}/(1-\gamma^2)$, a similarly renormalized interface specific resistance $AR_{F/N}$. The intrinsic quantity for the CPP-MR is the conductance per unit area, or its inverse, the specific resistance AR, where A is the area though which the current flows.

At cryogenic temperatures, where most of the data we review was taken, β is only uniquely defined for an F-alloy with a large enough concentration of a known impurity to dominate the scattering. In a nominally 'pure' F-metal, the scattering is dominated by residual impurities, grain boundaries, and stacking faults, all of which could vary with layer and total sample thicknesses, as well as with the method of sample preparation.

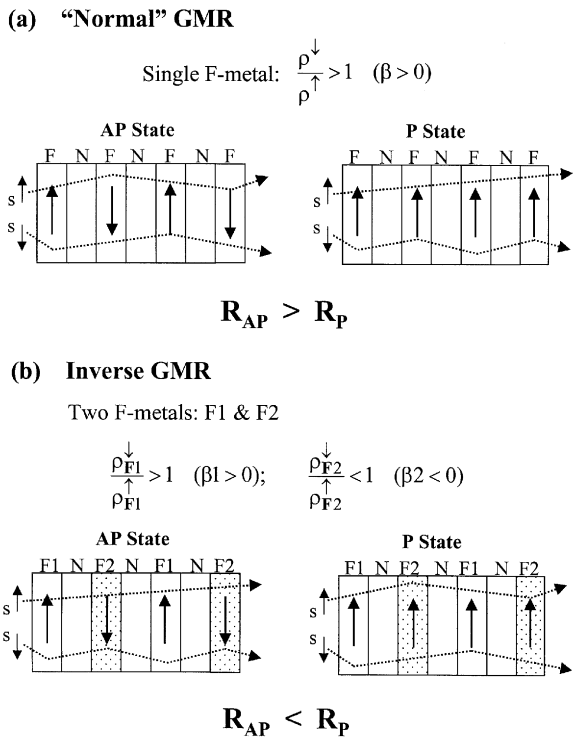

Fig. 4. Schematic drawings describing the physics underlying 'normal' and 'inverse' GMRs. (a) A single F-metal with $\beta > 0$ gives a normal MR [i.e., $R(AP) > R(P)$]. (b) Two F-metals with opposite signs of β give an inverse MR [$R(AP) < R(P)$]. The dotted lines indicate the paths of electrons with fixed spin-up or spin-down. The breaks in the lines indicate scattering events (strong scattering).

The situation for γ and $AR_{F/N}^*$ is even more complex, because they: (a) involve two different metals, F and N; (b) may vary with the structure of the interface – the amount of chemical roughness (alloying) or physical roughness (both correlated and uncorrelated, and on different length scales); and (c) may involve competition between contributions from alloying and potential steps [4,5,23–26] as well as between diffuse and specular reflection [23–26]. One, thus, needs to understand the sensitivities of γ and $AR_{F/N}^*$ to all varieties of roughness, and whether they are similar for the CIP- and CPP-MRs. It is not obvious that they should be, since a larger fraction of electrons impact the interfaces at small angles in the CIP-MR than in the CPP-MR, and spin-accumulation occurs at the

Table 1
Comparison of parameters for Co/Cu multilayers prepared in different ways. The analyses used values of AR either for the as-prepared state (H_0), or the peak state (H_{Pk})

	MSU [65] Sup. strips sputtering 4.2 K H_0	MSU [65] Sup. strips sputtering 4.2 K H_{Pk}	Leeds [66] Sup. strips MBE 4.2 K H_0	Doudin et al. [51] Nanowires electrodep. 20 K H_{Pk}	Piraux et al. [52,53] Nanowires electrodep. 77 K H_{Pk}	Co/Ag, MSU [36] Sup. strips sputtering 4.2 K H_0
ρ_{Cu} (nΩ m)	6 ± 1	6 ± 1	13 ± 3	13–33	~ 31	10 ± 3
ρ^*_{Co} (nΩm)	75 ± 5	66 ± 5	30 ± 6	510–570	180 ± 20	107 ± 10
β	0.46 ± 0.05	0.38 ± 0.06	0.48 ± 0.04	0.5 ± 0.08	0.36 ± 0.04	0.48 ± 0.05
γ	0.77 ± 0.04	0.71 ± 0.05	0.71 ± 0.02	0.3–0.6	0.85 ± 0.1	0.85 ± 0.03
$AR^*_{Co/Cu}$ (fΩ m^2)	0.51 ± 0.02	0.38 ± 0.03	0.43 ± 0.04	0.3–1.1	0.3 ± 0.05	0.56 ± 0.03

interfaces in the CPP-MR [4,14]. The CIP-MR seems to be sensitive to changing interfacial properties, but there is not yet agreement on the effects of the different contributions just noted (compare, e.g., the papers in Refs. [27–32]). For the CPP-MR, in contrast, evidence is sparcer, but tends to suggest less sensitivity (see Ref. [33] and Table 1). This difference is plausible, since perfectly specular interfacial scattering does not contribute to the CIP-MR, but can to the CPP-MR [4,5,23–26].

3.2. Spin relaxation at low temperatures

At cryogenic temperatures, electron–magnon scattering should be negligible, and $(+)$ and $(-)$ electron currents should not mix. This does not mean, however, that there are no characteristic lengths in spin-polarized transport.

In the CIP-MR, the $\uparrow$ and $\downarrow$ electron mean-free-paths, $\lambda^{\uparrow}$ and $\lambda^{\downarrow}$, in the F-layer, and λ^{N} in the N-layer, are all characteristic lengths. To know whether the sample is in the P or AP state, an electron starting in one F-layer must probe perpendicular to its drift direction far enough to encounter other F-layers, and an electron samples scattering only over a mean-free path from the center of its wave packet [4]. Because of structural anisotropies in the multilayers, these mean-free paths may be anisotropic [34]. The resulting equations for the CIP-MR are generally complex, containing exponential functions of the ratios of layer thicknesses to mean-free paths [4,34,35]. Any spin relaxation futher complicates the situation.

In the CPP-MR in contrast, to contribute to the current, electrons must pass through the entire multilayer and thus experience the difference between P and AP states, independent of their mean-free path(s). If there is no spin relaxation in the layers or at the interfaces, then the CPP-MR for single domain F-layers should be 'self-averaging' [4,8] – i.e., the mean-free paths drop out of the problem. The CPP-MR can then be described by a very simple two-current series-resistor (2CSR) model [8,14,22], summarized in Section 6. This model seems to be adequate for analyzing the CPP-MR of multilayers of 'pure' F-metals, such as Co, with N-layers in which spin-relaxation is weak [6,36]. If, however, spin-relaxation is strong enough so that the characteristic spin-diffusion length in either the F- or N-layers (l^{F}_{sf} or l^{N}_{sf}), or in both, becomes comparable to the respective layer thickness (t_F or t_N), CPP-MR analysis then requires the more complex equations of Valet and Fert (VF) [14]. The recent discovery that l^{Py}_{sf} in the technologically important alloy permalloy ($Py = Ni_{1-x}Fe_x$ with $x \sim 0.2$) is short [37–39], has led to awareness that finite l_{sf} can be important in multilayers of interest.

3.3. Current mixing at high temperatures

At temperatures high enough for electron–magnon scattering to become significant, the separate

(+) and (−) currents assumed above begin to mix. The parameters are the spin-mixing time, $\tau_{\uparrow\downarrow}$, or resistivity, $\rho_{\uparrow\downarrow}$. We will discuss later what has been learned about them, which is still very little.

4. Experimental techniques for CPP measurements

The quantities most appropriate for deriving fundamental parameters from the CPP-MR are usually AR(AP), AR(P), and their difference, $A\Delta R$. However, the CPP-MR $= A\Delta R/AR$(P) itself can sometimes allow simple analysis [40].

Three CPP techniques have been devised. Two, lithography [5,12,13] and electrodeposited nanowires [5,41–43,113], give resistances large enough ($>$ mΩ) for potential technology and allow measurements at room temperature. However, non-uniform currents in the lithographed samples [44] and, until recently [45,114], inability to determine the number of nanowires being measured, have limited these techniques to providing the CPP-MR rather than $A\Delta R$. So far, electrodeposition is also limited to just a few metals, and to only one F-alloy and one N-alloy at a time; flexible control of the AP state has thus yet to be achieved. The only technique that has directly given $A\Delta R$ in multilayers involves the use of crossed superconducting strips to produce uniform current density [9]. With either sputtering or MBE, this technique allows the complex combinations of metals needed for flexible control of the AP and P states (Section 5). However, the use of superconducting strips is limited to low temperature. Moreover, samples with macroscopic areas, $A \sim \text{mm}^2$, have resistances $\leqslant 10^{-7}\,\Omega$, too small for devices. Fortunately, low temperature is advantageous for deriving most parameters and testing basic understanding, since it eliminates the complicating effects of scattering of electrons by magnons (which mixes spin currents) and by phonons. For details of the techniques for measuring the CPP-MR, and their problems, see Ref. [5]. Refs. [46–50] describe multilayers deposited into angled grooves, giving current at an angle to the plane (CAP). The CPP-MR can be estimated from a combination of CIP- and CAP-MRs [50].

5. Producing AP and P states

As has recently been emphasized [7], reliable determination of $A\Delta R$ requires control of both the AP- and P-states. The P-state can be reached simply by increasing the external field H to above the saturation field(s), H_s, of the F-metal(s). The AP-state is, however, harder to achieve for wide ranges of thicknesses of both the F- and N-metals. For simple $[F/N]_N$ multilayers, several alternatives have been used to approximate R(AP) in the CPP-MR: (a) $R(0)$, the resistance of the as-prepared sample (Fig. 1) [22]; (b) R(Pk), the maximum $R(H)$ after saturation (Fig. 1) [51–53]; (c) an R(Pk) 'corrected' based on magnetic force microscope studies [40]; (d) the larger of $R(0)$ or R(D) (the resistance after demagnetization) [54]; and (e) use of two different thicknesses of the N-layer [55]. More reliable control for a wide range of layer thicknesses can be achieved using two techniques first developed for the CIP-MR, hybrid-SVS [56] and exchange-biased SVs (EBSVs) [57,58]. These two techniques now permit controlled CPP-studies.

A hybrid-SV (top of Fig. 5) is an $[F1/N/F2/N]_N$ multilayer composed of metals F1 and F2 with very different saturation fields, $H_{s1} \gg H_{s2}$. Increasing H to above H_{s1} will produce the P state, and then reversing H to just beyond '$-H_{s2}$' should produce the AP-state (provided the remanent magnetization of F1 is close enough to its saturation value that the $\boldsymbol{M}_i$'s of the F1 layers do not decrease significantly by $-H_{s2}$). Fig. 5 [59,60] shows $M(H)$ and CPP-MR(H) for a hybrid SV. A close approximation to the AP state is usually found only over a narrow range of H.

An EBSV has the form [AF/F1/N/F2], where AF is an appropriate antiferromagnetic (AF) metal, and F1 and F2 can be the same or different metals. Heating and cooling the sample in the presence of a magnetic field can 'exchange bias' F1 (the F-metal next to the AF-metal), so that its hysteresis loop is shifted away from $H = 0$ [57,58]. If the N-layer is thick enough so that exchange coupling between F1 and F2 is weak, F2 will still be free to reorient in a smaller field, H_{s2}. Fig. 6 [37–39,61] shows M and CPP-MR for a [FeMn/Py/Cu/Py] EBSV. EBSVs can give a well-defined AP state over a finite range of H. However, the pinning field decreases as $1/t_{F1}$,

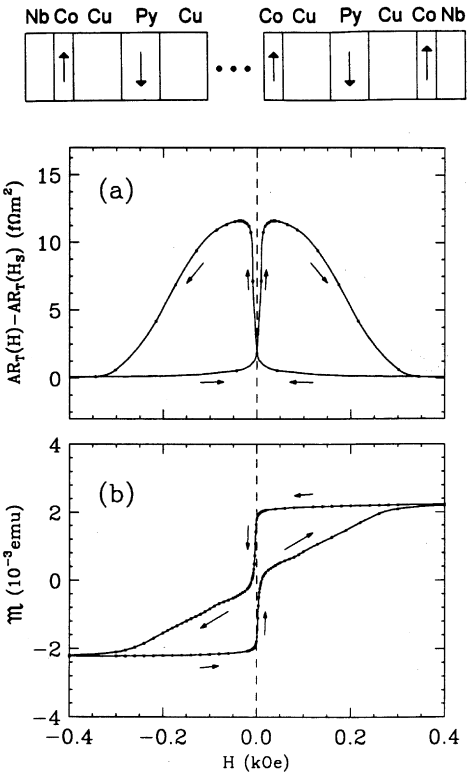

Fig. 5. Change in: (a) specific resistance, $AR(H) - AR(P)$, and (b) magnetization, M, for a Co/Cu/Py/Cu hybrid spin valve, shown schematically at the top of the figure. The curves are just guides to the eye (from Ref. [59]).

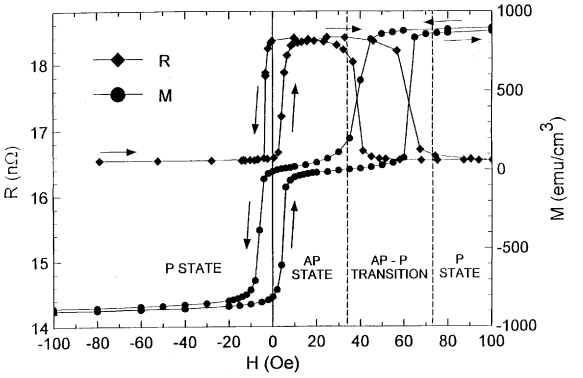

Fig. 6. Resistance (R) (diamonds and left scale) and magnetization M (circles and right scale) versus applied field for an [FeMn/Py/Cu/Py] exchange-biased spin valve. The parallel (P) and anti-parallel (AP) magnetic states are indicated below the curves, which are just guides to the eye. The agreement of the values of R for the oppositely oriented P states shows that the FeMn does not participate directly in the MR (from Ref. [61]).

so the ability to maintain an AP state diminishes as t_{F1} grows.

6. Theory and tests thereof

The equations used to analyze CPP-MR data assume that the sources of GMR can be divided into 'bulk' and 'interfacial'. This assumption has been questioned [4,5,23–26], but no data yet contradict it.

Zhang and Levy [8] first argued that, at temperatures where electron–magnon scattering is negligible, the mean-free paths ($\lambda^{\uparrow}$, $\lambda^{\downarrow}$, λ^{N}) should drop out of the CPP-MR, making it 'self-averaging' – i.e., having no length scale. The CPP-MR can then be described by a very simple two-current series-resistor (2CSR) model described below [14,22]. This model seems to work well most of the time in simple multilayers such as $[Co/Cu]_N$ and $[Co/Ag]_N$ [6,36].

Valet and Fert (VF) [14] soon pointed out that the 2CSR model should not always be valid. There are characteristic lengths in the CPP-MR, the spin-diffusion lengths l_{sf}^{F} and l_{sf}^{N}, over which spins relax as the electrons traverse the sample. When l_{sf}^{F} or l_{sf}^{N} become comparable to t_F or t_N, more complex equations are needed [14]. Originally, spin relaxation was expected to be weak, and corrections for finite l_{sf} small. We will see, however, that l_{sf} can be short enough to produce large changes in $A\Delta R$, sometimes so short that it is not clear that the VF equations remain valid. The VF equations are strictly only the 'local' terms in a Boltzmann equation analysis, with non-local corrections $\sim \lambda/l_{sf}$ that are negligible only if $\lambda/l_{sf} \ll 1$ [14].

6.1. The 2CSR model

This model assumes that the spin-anisotropy parameters β and γ defined above are independent of t_F, t_N, and N. For a simple $[F/N]_N$ multilayer with superconducting (S) leads, including

a spin-independent interface specific resistance, $AR_{S/F}$, for each S-lead, gives [22]

$$AR(\mathrm{AP}) = 2AR_{S/F} + 2N\rho_N t_N + N\rho_F^* t_F + 2NAR_{F/N}^*, \quad (2)$$

$$A\Delta R = N^2[\beta\rho_F^* t_F + 2\gamma AR_{F/N}^*]^2/AR(\mathrm{AP}). \quad (3)$$

For simplicity, we neglect differences between N, $N-1$, and $N+1$.

Together, Eqs. (2) and (3) contain six parameters, $AR_{S/F}$, ρ_N, ρ_F^*, $AR_{F/N}^*$, β, and γ. For sputtered samples, a number of papers (e.g., Refs. [6,22,36]) have shown that consistent results can usually be obtained on CPP-MR multilayers and CPP-SVs assuming independently determined values of $AR_{S/F}$, ρ_N and ρ_F (only occasionally has this assumption seemed to break down [36,62]). $AR_{S/F}$ is taken to be the ordinate intercept of a linear fit to AR versus t_F for a series of S/F(t_F)/S trilayers, and ρ_N and ρ_F are taken to be the resistivities measured on thick films of the same metals prepared in the same way as the multilayers or SVs. When this assumption applies, the number of adjustable parameters reduces to only three, $AR_{F/N}^*$, β, and γ, few enough to be determined experimentally by measuring AR(AP) and $A\Delta R$ for samples with ranges of t_F and t_N [6,36]. As noted above, the major experimental problem is to achieve AP states for this range of thicknesses. Some studies have approximated the AP state by the state R(Pk) in Fig. 1a, because R(Pk) is reproducible in a given sample. We have argued that a better approximation is $R(0)$ [22,63], an argument now supported by a combination of polarized neutron reflection (PNR) and scanning-electron-microscopy with polarization analysis (SEMPA) [64]. Both $R(0)$ and R(Pk) provide estimates of $AR_{F/N}^*$, β and γ. Table 1 [36,51–53,65,66] compares values for $[\mathrm{Co/Cu}]_N$ multilayers prepared by sputtering, MBE, and electrodeposition, obtained with $R(0)$ or R(Pk). Equivalent values for Co/Ag for $R(0)$ are included for comparison. As expected from Fig. 2 plus Eq. (3), the estimates of β, γ and $AR_{F/N}^*$ for R(Pk) are lower than those for $R(0)$. In addition, since β is determined by the scattering defects in the F-layers, and γ and $AR_{F/N}^*$ may depend upon the chemical (i.e., alloying) and physical (e.g., geometrical roughness) structures of the interfaces, it seems unlikely that the values for different preparation techniques will be identical. It is thus both somewhat surprising, and apparently evidence for insensitivity of the CPP-MR to structural details, that the different sets of parameters in Table 1 are so similar. The differences between the values of ρ_{Co}^* and β for Co derived for Co/Cu and Co/Ag samples prepared in the same laboratory indicate present limiting uncertainties.

Eqs. (2) and (3) allow tests of the 2CSR model that are independent of the particular values of the parameters. Applying each to a set of samples with fixed total thickness $t_T = N(t_F + t_N)$, allows t_N to be eliminated. For example, if t_F is kept fixed and N varied, Eq. (2) can be written as the sum of terms proportional to N plus the constant term $AR_{S/F} + \rho_N t_T$. This equation was used to show the validity of replacing $AR_{S/F}$ and ρ_N by their independently measured values [22]. Eq. (3) can be rewritten to show that a plot of $\sqrt{[AR(\mathrm{AP}) - AR(\mathrm{P})]AR(\mathrm{AP})}$ versus N should yield data that fall on a straight line passing through the origin, with slope *independent* of both ρ_N and t_T [22]. Fig. 7 [67] illustrates the validity of such a plot for multilayers of $[\mathrm{Co}(6\ \mathrm{nm})/\mathrm{Ag}(t_{Ag})]_N$ and $[\mathrm{Co}(6\ \mathrm{nm})/\mathrm{AgSn}(t_{AgSn})]_M$ with $t_T = 720$ nm, as well as for $[\mathrm{Co}(6\ \mathrm{nm})/(\mathrm{Ag}(6\ \mathrm{nm})]_N$ multilayers [22,68]. Note that $\rho_{AgSn} \approx 20\rho_{Ag}$ and that N ranges from 1.5 to 60.

As a quantitative test, the values of β, γ and $AR_{F/N}^*$, derived for Co/Cu and Py/Cu multilayers, were used to predict data for a series of sputtered $[\mathrm{Co/Cu/Py/Cu}]_N$ hybrid SVs [59,60]. The equation is then [69]

$$A\Delta R = 4N^2[\beta_1\rho_{F1}^* t_{F1} + 2\gamma_1 AR_{F1/N}^*] \times [\beta_2\rho_{F2}^* t_{F2} + 2\gamma_2 AR_{F2/N}^*]/AR(\mathrm{AP}). \quad (4)$$

AR(AP), AR(P), and $A\Delta R$ were all reasonably well predicted without adjustment [59,60]. This agreement engendered confidence in the transferability of parameters between simple $[\mathrm{F/N}]_N$ multilayers and hybrid SVs or EBSVs, at least for samples prepared in the same laboratory. Assuming such transferability, once the parameters for a given F1/N pair are known, hybrid SVs can be used to determine the parameters for another pair, F2/N. Note that if only β_2 is negative, the MR will be

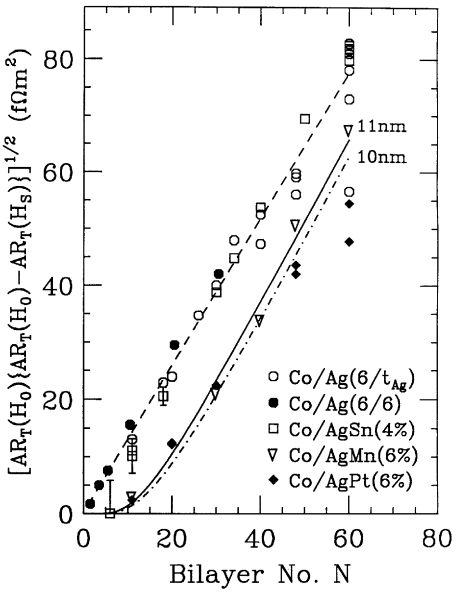

Fig. 7. $\sqrt{[AR(0)-AR(\mathrm{P})]AR(0)}$ versus bilayer number N for $[\mathrm{Co}(6\ \mathrm{nm})/\mathrm{X}(t_x)]_N$ multilayers with fixed total thicknesses of 720 nm, except for the samples indicated by filled circles, which had the form $[\mathrm{Co}(6\ \mathrm{nm})/\mathrm{Ag}(6\ \mathrm{nm})]_N$. The spin-diffusion lengths for the Co/Ag and Co/AgSn multilayers were long enough so that the data remained (to within uncertainties) on the straight line passing through the origin predicted by Eq. (3). The spin-diffusion lengths for the AgMn and AgPt samples were short enough to cause deviations from this line. The solid and broken curves passing through the latter data are fits using the theory of VF [14]. The resistivities of the alloys, and the deduced values of l_{sf}^{N} are given in Table 2 (from Ref. [67]).

inverse for thick enough t_2, and if only γ_2 is negative, the MR will be inverse for very thin t_2.

Lastly, $A\Delta R$ in the 2CSR model for an EBSV [AF/F/N/F] is

$$A\Delta R = 4(\beta\rho_F^* t_F + \gamma AR_{F/N}^*)^2/AR(\mathrm{AP}), \tag{5}$$

where

$$AR(\mathrm{AP}) = AR_{S/F} + 2\rho_F^* t_F + \rho_N t_N + 2AR_{F/N}^* + AR_{AF/F} + \rho_{AF} t_{AF} + AR_{S/AF}.$$

6.2. The Valet–Fert (VF) model

It was always realized that the 2CSR model would break down when the temperature T became high enough for electron–magnon scattering to mix the (+) and (−) spin currents. But Valet and Fert (VF) [14] first noted that spin-flip processes that do not mix spin currents could affect the CPP-MR even at low T. Current mixing involves the transfer of momentum (and thus current) between the spin-up (+) and spin down (−) channels. The new phenomenon, spin diffusion (or spin relaxation) does not. Rather, it leads to a phenomenon called spin accumulation at interfaces, previously investigated for single interfaces or simple sandwiches in Refs. [70,71]. VF showed that the CPP-MR has characteristic spin-diffusion lengths in the F- and N-metals defined by $l_{sf} = \sqrt{(\lambda_{el}\lambda_{sf})}/6$, where λ_{el} is the momentum relaxing mean-free path and λ_{sf} the spin mean-free path [14,72]. In the limit that l_{sf}^{F} and l_{sf}^{N} are both $\gg \lambda_{el}^{F}$, λ_{el}^{N}, but l_{sf}^{F} and l_{sf}^{N} become comparable to t_N and t_F, VF showed how to generalize Eqs. (2) and (3). When l_{sf}^{N} and l_{sf}^{F} are both comparable to t_N and t_F, the VF equations can be almost as complex as those for the CIP-MR. When only one (e.g., l_{sf}^{F}) is comparable to its layer thickness (t_F), only one new variable, (l_{sf}^{F}), must be added to the 2CSR model, but the presence of exponentials of the form $\exp(-t_{F/}l_{sf}^{F})$ now generally requires a numerical solution. Interestingly, when $l_{sf}^{F} < t_F$, the VF equation for $A\Delta R$ simplifies in an unusual way. For example, for an [AF/F/N/F] EBSV with $l_{sf}^{F} < t_F$, one finds just

$$A\Delta R = 4[\beta\rho_F^* l_{sf}^{F} + \gamma AR_{F/N}^*]^2/ [2\rho_F^* l_{sf}^{F} + 2AR_{F/N}^* + \rho_N t_N]. \tag{6}$$

Note that the denominator in Eq. (6) reduces to just the AR in the MR 'active' region, the outer boundaries of which lie within the F-layers at a distance l_{sf}^{F} from the two F/N interfaces. Comparing Eqs. (5) and (6) shows that a larger decrease in the denominator than in the numerator could cause $A\Delta R$ to increase as l_{sf} decreases.

Eqs. (4)–(6) form the basis of most of the analyses of new data in the following sections.

7. β CPP-MR, including comparisons with β for dilute F-alloys

The first quantitative CPP-MR estimate of β for an F-alloy was the value of $\beta_{Py} \sim 0.5$ in Py (NiFe)

derived assuming that $l_{sf}^{Py} = \infty$ [73]. The subsequent discovery of a finite l_{sf}^{Py} led to an increase in this estimate to $\beta_{Py} \approx 0.7 \pm 0.1$ [37–39,65], a value that overlaps the range of values $0.76 \leqslant \beta_{NiFe} \leqslant 0.9$ listed for dilute NiFe in Campbell–Fert [20].

An important qualitative test of the Campbell–Fert tables was made in Refs. [15–17]. There, four different alloys with expected negative β's – FeCr, FeV, NiCr, and CoCr – were combined with very thin Co layers (granular-Co) into hybrid-SVs, which were then used to search for 'inverse' CPP-MRs when the alloy layer thicknesses were large enough to overcome their 'normal' interface contributions (see Eq. (4)). The very large H_s of granular Co was intended to ensure a good AP state. Fig. 8 shows several examples of the CPP-MRs changing from normal to inverse with increasing alloy thickness. Interestingly, in none of the samples did the CIP-MR became inverse. This difference in behaviors seems clear evidence that interfacial scattering is relatively more important in the CIP-MR than in the CPP-MR. While the changes from normal to inverse MR in Fig. 8 are heartening evidence of qualitative similarity of CPP-MR and alloy values of β, the values of $\beta \sim -0.1$ estimated from the CPP-MR [15,16] are much less than the Campbell–Fert values of $\beta \sim -(0.4-0.5)$. The uncertainties in the CPP-MR estimates are large, both because the parameters assumed for granular-Co have not been independently established, and because the data analysis assumed $l_{sf}^{F} = \infty$ for all of the F-alloys. Thus, a more detailed study of NiCr was undertaken, against Py, for which the parameters are better known than granular-Co. Allowing for a finite l_{sf}^{NiCr}, gave $\beta_{NiCr} = -0.35 \pm 0.1$, close to the Campbell–Fert range $-0.38 \geqslant \beta_{NiCr} \geqslant -0.67$ [18].

Among Co-based alloys, the largest β in the Campbell–Fert list is $\beta_{CoFe} = 0.85 \pm 0.1$. Fig. 9, from a recent study of [FeMn/$Co_{0.91}Fe_{0.09}$/Cu/$Co_{0.91}Fe_{0.09}$] EBSVs [18], shows that $A\Delta R$ is indeed much larger than for [FeMn/Co/Cu/Co] EBSVs. The apparent saturation of the data for large t_{CoFe} strongly suggests a finite l_{sf}^{CoFe}. The solid curve is the VF fit for $\beta_{CoFe} = 0.65 \pm 0.05$ (comparable to, but smaller than, the Campbell–Fert value of $\beta_{CoFe} = 0.85 \pm 0.1$) and $l_{sf}^{CoFe} = 12 \pm 1$ nm.

Finally, a half-metallic metal, in which either $\rho^{\downarrow} = \infty$ or $\rho^{\uparrow} = 0$ should give CPP-MR $= \infty$. The Heusler alloy NiMnSb has been predicted to be half-metallic [74], but independent measurements of electronic structure do not support this prediction [75]. Measurements of samples with NiMnSb have so far yielded disappointingly small CPP-MRs [76]. Whether the problem is fundamental,

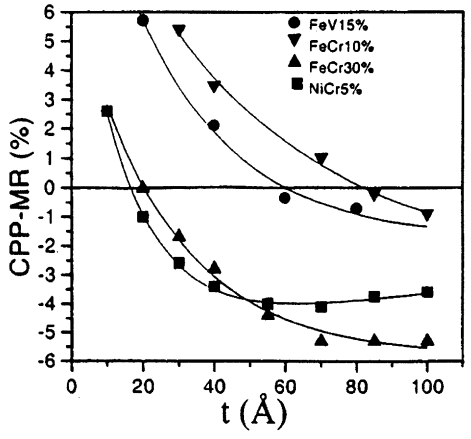

Fig. 8. CPP-MR versus t for [Co(0.4 nm)/Cu(2.3 nm)/X(t)/Cu(2.3 nm)]$_{20}$ multilayers showing inverse MR for thick enough layers of X = FeV (15%), FeCr (10%), FeCr (30%), and NiCr (5%). The solid curves are just guides to the eye (from Ref. [16]).

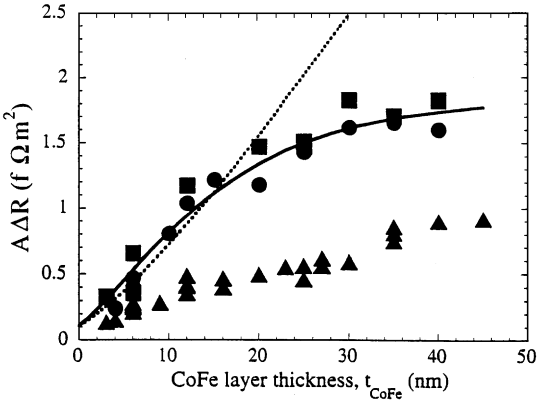

Fig. 9. $A\Delta R$ versus t_{CoFe} (circles and squares) or versus t_{Co} (triangles) for [FeMn/X(t_x)/Cu(20 nm)/X(t_x) EBSVs with X = CoFe or Co. The circles and squares indicated different series of samples prepared months apart. The solid curve is a fit to the theory of VF [14] with $l_{sf}^{CoFe} = 12$ nm. The dashed curve is the 2CSR model prediction for the same parameters as for the solid curve, except $l_{sf}^{CoFe} = \infty$ (from Ref. [86]).

or due to inadequate quality of the sputtered NiMnSb, must still be determined.

To summarize, so far, the values of β for dilute alloys derived from the CPP-MR are mostly comparable to, but slightly smaller than, those listed by Campbell and Fert. Studies of more alloys are needed to test the relationship more widely.

8. γ-CPP

γ-CPP has been determined explicitly for only a few interfaces, Co/Cu (Table 1), Co/Ag ($\gamma = 0.85 \pm 0.03$ [36]), and Py/Cu ($\gamma = 0.7 \pm 0.1$ [37–39,77]). The close agreement between data for Co/Ag and Co/AgSn shown in Fig. 7 suggests that γ for Co/AgSn is close to that for Co/Ag. Unless adding a small amount of an impurity induces large changes in the electronic structure of N, it seems reasonable that γ for F/N′, where N′ is a dilute alloy of N, will be almost the same as that for F/N.

The general similarity of values of γ in Table 1 for Co/Cu multilayers prepared and measured in very different ways suggests that γ in the CPP-MR is not very sensitive to structural changes. The only direct CPP-MR study so far [33] of deliberately induced changes in interfacial structure also indicates only modest effects.

As noted in Section 7, the Campbell–Fert tables list negative β's for dilute FeCr and CoCr alloys, and CPP-MR measurements support such values. Fe/Cr and Co/Cr interfaces might then be expected to have negative values of γ [78]. Indeed, measurements of $[X/Cr/Py/Cr]_N$ hybrid SVs with X = Fe and Co gave inverse $A\Delta R$ for thin Fe or Co layers, but normal $A\Delta R$ when the layers became thicker [17]. This is the behavior expected if β is positive within 'pure' Fe or Co, but γ is negative at the Fe/Cr or Co/Cr interface.

9. Interface specific resistances, including $AR^*_{F/N}$ or $AR_{F/N}$

Also still little understood is the interface specific resistance $AR^*_{F/N}$ (or $AR_{F/N}$). $AR^*_{F/N}$ is expected to contain contributions from interfacial alloying, scattering from spin-dependent potential steps at the interface, and perhaps from scattering from interfacial states [4,5,23–26]. Contributions from diffuse and specular scattering may also interact [23–26]. Few experiments distinguish between these possibilities.

$AR^*_{F/N}$ has been measured so far only for Co/Ag, Co/Cu, and Py/Cu (Table 1, Refs. [37–39,67]). In all three cases, its value is ~ 0.5 fΩ m^2. The estimated values of γ for these three pairs differ enough so that the values of $AR_{F/N} = AR^*_{F/N}(1-\gamma^2)$ spread somewhat more ($0.16 \leqslant AR_{F/N} \leqslant 0.25$) The agreement of data for Co/Ag and Co/AgSn in Fig. 7 and [79] suggests that adding small amounts of an impurity probably usually has little effect on $AR_{F/N}$.

To remove complications of the two-current model, AR_{N_1/N_2} was recently studied in noble-metal/noble metal multilayers [80]. To within substantial uncertainties, the magnitudes of AR_{N_1/N_2} (0.044–0.15 fΩ m^2) could be attributed just to alloying at the N_1/N_2 interfaces.

Reported values of $AR_{S/F}$ are mostly considerably larger: ~ 3 fΩ m^2 for Nb/Co, ~ 2.4 fΩ m^2 for Nb/Ni, 6 fΩ m^2 for NbTi/Co [81]. The only estimate for $AR_{S/AF}$ is intermediate, $AR_{Nb/FeMn} = 1.0 \pm 0.6$ fΩ m^2 [37–39].

$AR_{AF/F}$ has also been estimated: $AR_{FeMn/Py} = 1.0 \pm 0.4$ fΩ m^2 [37–39] and $AR_{FeMn/Co} = 0.6 \pm 0.3$ fΩ m^2 [62].

Spin-dependent potential steps at interfaces have been predicted to produce deviations from a linear variation of the CPP-MR with the cosine of the angle between the magnetizations of adjacent F-layers [82]. Deviations from linearity have been found, but in one case the use of two different F-metals [83], and in the other different deviations for different values of t_F [84], leave the interpretations, and thus the source(s) of these deviations, unclear.

10. Finite spin-diffusion lengths

The fundamental length in the CPP-MR at low temperatures is the spin-diffusion length, l_{sf}. For ease of discussion, we treat the experimental results out of historical order. We start with l^F_{sf} in F-metals and alloys, then turn to l^N_{sf} in N-metals and alloys, and conclude with data on spin relaxation

at interfaces. The temperature dependence of l_{sf}^{Co} will be covered in Section 11.

10.1. F-metals and F-alloys

We already noted the unexpected discovery of a short l_{sf} in Py ($l_{sf}^{Py} = 5.5 \pm 1$ nm [37–39]), a value that has recently received independent support [85]. In contrast, the l_{sf} in Co appears to be much longer [40], in fact long enough so that the simple 2CSR model can be applied to $[Co/Cu]_N$ and $[Co/Ag]_N$ multilayers with t_{Co} up to about 50 nm [36,62]. In contrast, recent EBSV studies of $Co_{91}Fe_9$ [86] and $Ni_{97}Cr_3$ [87] suggest values of l_{sf} closer to that of Py. Data and a fit for CoFe were shown in Fig. 9. Interestingly, the values of l_{sf} for Py (NiFe), CoFe, and NiCr scale almost linearly with the inverse of their residual resistivities (Fig. 10). The l_{sf} for Co, however, falls well above this line. Further studies are needed to discover if this difference means that the correlation of Fig. 10 is accidental, or if the probability of spin-flip scattering by grain boundaries and stacking faults is quite different from that for impurities.

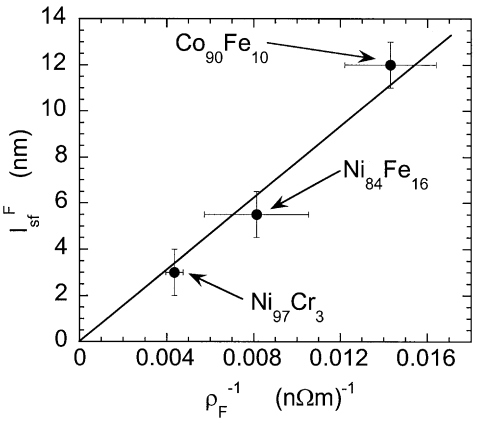

Fig. 10. l_{sf}^{F} versus $(1/\rho_F)$ for $Ni_{84}Fe_{16}$ (Py) [37–39], $Co_{90}Fe_{10}$ [86], and $Ni_{97}Cr_3$ [87]. The values of l_{sf}^{F} were derived by applying the VF theory to EBSVs with equal thicknesses of the pinned and free layers.

10.2. N-metals and N-based alloys

The first evidence of finite l_{sf} in nominally pure N-metals was obtained by Johnson and Silsbee, using a spin-injection technique [70,88]. They inferred low-temperature values of $l_{sf}(Al) \sim 200$–400 μm for injection into a 50 μm thick, annealed Al bar [70], and $l_{sf}(Au) = 1.5 \pm 0.4$ μm for evaporated films [88]. The CPP-MR was first used to derive values of l_{sf} in alloys [89] based upon Eq. (3) and its generalization by VF. Because the right-hand side of Eq. (2) is independent of ρ_N, alloying an N-metal with impurities that do not induce spin relaxation, should give the same value of $\sqrt{[AR(AP) - AR(P)]AR(AP)}$ as for the pure N-metal. Such behavior was illustrated in Fig. 7 for AgSn [22]. If, however, adding impurities causes spin relaxation between F-layers, $\sqrt{[AR(AP) - AR(P)]AR(AP)}$ should decrease, with the data in Fig. 7 falling below the straight line by a larger fraction the stronger the spin relaxation and the larger t_N (i.e., the smaller N). Data are shown for Pt (strong spin-orbit interaction) and Mn (strong spin-exchange interaction) in Ag [67,89]. The solid and broken curves are fits to the VF equations. As shown in Table 2, the inferred values of l_{sf}^{N} for Sn, Pt, and Mn in Ag and Pt, Mn, and Ni [90] in Cu, all agree rather well with estimates from spin–orbit and spin–spin interactions [72,89]. More recently, values of l_{sf}^{Cu} for Cu with residual Co impurities in electrodeposited Co/Cu multilayers have been estimated to range from 140 nm [91] up to 450 nm [92] in different sample sets.

The main problem with all of these studies is that there is no guarantee that the samples had reached the AP state needed for rigorous analysis. This difficulty can now be overcome by using the 'spin-relaxation-analyzer' EBSV, shown at the top of Fig. 11, where $t_{Py} = 24$ nm is chosen $\gg l_{sf}^{Py}$ so that Eq. (6) should apply. Here, the insert 'I' to be measured is placed in the center of the Cu layer in an [FeMn/Py/Cu/Py] EBSV with total Cu thickness large enough (~ 20 nm) to magnetically decouple the pinned and free Py layers. 'I' may consist of just a single layer of variable thickness, t_I, or a multilayer of two different metals, N_1 and N_2, with fixed thicknesses but variable number of bilayers N (thus $2N$ interfaces). If 'I' does not induce spin relaxation, $A\Delta R$ will decrease algebraically with increasing t_N or N, as $\rho_I t_I$ or $2NAR_{N_1/N_2}$ contributes to the denominator of Eq. (6). If,

Table 2
Measured [80,82] and calculated [80,82,83] values of l_{sf}^{N} for Cu- and Ag-based alloys

Metal or alloy	ρ (nΩ m)	l_{sf}^{N} (measured)	l_{sf}^{N} (calculated)
Ag	9 ± 1	Long	~ 500 nm
AgSn (4 at%)	200 ± 20	$\geqslant 26$ nm	~ 26 nm
AgMn (6 at%)	110 ± 25	~ 11 nm	~ 12 nm
AgMn (9 at%)	155 ± 20	~ 7 nm	~ 9 nm
AgPt (6 at%)	110 ± 20	~ 10 nm	$\geqslant 7$ nm
Cu	6 ± 1	Long	~ 450 nm
CuMn (7 at%)	270 ± 30	~ 3 nm	~ 3 nm
CuPt (6 at%)	130 ± 10	~ 8 nm	~ 7 nm
CuNi (7 at%)	110	~ 23 nm	~ 22 nm
CuNi (23 at%)	355	~ 7.5 nm	~ 7 nm

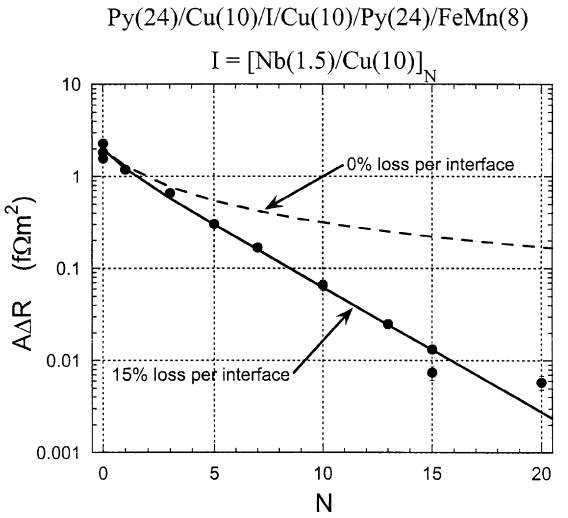

Fig. 11. Log($A\Delta R$) versus bilayer number N (i.e. $2N$ interfaces) for a spin-memory loss analyzer with insert 'I' (top of figure). All distances in the figure are in nm, and for symmetry with this particular insert, 'I' = [Nb(1.5 nm)/Cu(10 nm)]$_N$, the last Cu(10 nm) layer was omitted. The dashed curve indicates the decrease in $A\Delta R$ expected for no-spin-memory loss (i.e., due only to the increase in total resistance produced by the insert). The solid line is a fit to the data using the VF theory with a spin-memory loss of $\sim 15\%$/interface (after Ref. [94]).

however, 'I' induces spin relaxation, $A\Delta R$ will decrease exponentially as $\exp(-t_I/l_{sf}^{N})$ or $\exp(-N)$ in the numerator. Such behavior has been tested with I = [Cu/Ag]$_N$ multilayers, for which the interface resistance is small [80] and the electronic structures of the metals are so similar that little spin relaxation is expected. Any relaxation was indeed small, less than 0.5%/interface [93]. In contrast, Fig. 11 shows an unexpectedly large spin relaxation ($\sim 15\%$/interface) recently discovered in I = [Nb/Cu]$_N$ [94]. The source of this relaxation is not yet known, but it may result from strong spin–orbit scattering in an unusually high resistivity (~ 1500 nΩ m [95]) NbCu alloy formed at the interface.

11. Temperature variation of CPP-parameters and spin mixing

The data described in the previous three sections were all taken at 4.2 or 77 K (e.g., Table 1), where little temperature dependence is expected for such 'dirty' metallic multilayers (i.e. containing so many defects). For both physics and technology, it is important to understand how the CPP-MR changes at higher temperatures. Neglecting spin mixing, and changes in β, γ, and $AR_{F/N}^{*}$ with T, Eq. (3) predicts that $A\Delta R$ should increase with increasing T, since the resistivity in the numerator is squared. In Co/Cu multilayers (Fig. 3a) and [Co/Cu/Py/Cu] hybrid SVs [96], the CPP-MR decreases by only about 20% from 4 to 300 K, whereas the sample resistance AR can increase by a factor of two or more [96]. Combining these results requires that $A\Delta R$ must increase with T. More detailed analysis of Co/Cu multilayers suggests that β may decrease slightly (from ~ 0.4 at 4.2 K to ~ 0.3 at 300 K), and that spin mixing in Co/Cu is relatively modest even at 300 K (e.g., $\rho_{\uparrow\downarrow} \sim 40$ nΩ m compared to an estimated $\rho_{Co} \sim 250$ nΩ m) [40]. In Fe/Cr, in contrast, the MR drops by a much larger fraction (Fig. 3b), more than the typical factor of two increase in R, suggesting that spin mixing is much stronger.

12. Some new directions

New directions for CPP-MR studies include studies of ballistic transport, point contacts, very high current densities, and transport of 'hot' electrons (i.e. electrons away from the Fermi energy).

All of the analyses above used models appropriate to diffusive transport. Interfacial effects predicted to be associated with ballistic transport

[97–99] have been looked for with point contacts [100] or macroscopic samples [101], but not yet seen. Information about anisotropic ballistic transport across S/F interfaces has just been derived from studies of Andreev reflection with point contacts [102].

Evidence for predicted effects of very high current densities [103–105] has been reported [106].

Studies of transport of 'hot' electrons through magnetic multilayers are now being made both with macroscopic samples [107,108] and point contacts [109,110].

13. Summary and some questions

To summarize, the CPP-MR is typically larger than the CIP-MR, and usually described by simpler equations that allow more direct access to the fundamental parameters of spin-polarized transport. The use of hybrid-spin valves and exchange-biased spin valves (EBSVs) to control magnetic order is beginning to allow these fundamental parameters to be determined. In this review we have described what has been learned so far about: β – the bulk anisotropy parameter in the F-layer; γ – the F/N interface anisotropy parameter; $AR^{*}_{F/N}$ – the F/N interface specific resistance; l^{F}_{sf} and l^{N}_{sf} – the spin-diffusion lengths in the F- and N-layers; and spin mixing at higher temperatures.

We conclude with several experimental or theoretical questions that are not yet fully resolved.

(1) Why does the two-current series-resistor (2CSR) model for the CPP-MR work so well when l^{F}_{sf} and l^{N}_{sf} are longer than t_F and t_N? It is not clear that the following assumptions in its application are all necessarily valid: (a) bulk and interface contributions to AR(AP) are simply additive; (b) all parameters are independent of t_F, t_N, and total sample thickness t_T; and (c) parameters such as ρ_N and ρ_F can be replaced by independently measured values.

(2) Are the Valet–Fert (VF) equations still valid under all of the conditions where they have been applied, even those where l_{sf} is apparently not much longer than the elastic mean-free path?

(3) Are values of β for the CPP-MR and dilute alloys always similar?

(4) What are the relative contributions to $AR_{F/N}$ and γ from interfacial alloying, potential steps, and geometrical roughness (and what roughness length scales predominate)?

(5) What determines the temperature dependence of the CPP-MR parameters, and how large is spin mixing?

(6) In Eq. (1), $AR_{S/F}$ has been included as a spin-independent, additive term. Is this correct for this diffusive regime? It has just been argued that S-leads suppress the CPP-MR in a phase-coherent multilayer [111].

(7) What determines l^{F}_{sf} and l^{N}_{sf}? For non-magnetic hosts and non-magnetic impurities, the published data are consistent with dominance of spin–orbit relaxation [72,89]. Spin–orbit relaxation has also been proposed to dominate magnetic hosts [85]. l^{N}_{sf} for alloys with magnetic impurities is less well understood [72,89], with published data only for AgMn and CuMn [89].

(8) How strong is spin relaxation at F/N and other interfaces? What is the underlying physics?

(9) Are there important experimental differences between diffusive and ballistic spin-polarized transport? For the most recent calculation addressing this issue see [112].

Acknowledgements

This work was supported in part by the MSU CFMR, by Ford Research Laboratories, and by the US NSF under grants DMR 94-23795 and MRSEC DMR-94-00417 and 98-09688. The authors thank their students and collaborators for crucial contributions to many of the results described in this review, and especially P.A. Schroeder, who also made helpful suggestions for this manuscript.

References

[1] M.N. Baibich et al., Phys. Rev. Lett. 61 (1988) 2472.
[2] G. Binash et al., Phys. Rev. B 39 (1989) 4828.
[3] J.A. Brug et al., J. Appl. Phys. 79 (1996) 44991.

[4] P.M. Levy, in: H. Ehrenreich, D. Turnbull (Eds.), Solid State Physics Series, Vol. 47, Academic Press, New York, 1994, p. 367.
[5] M.A.M. Gijs, G. Bauer, Adv. Phys. 46 (1997) 285.
[6] J. Bass et al., Comments Cond. Matt. Phys. 18 (1998) 223.
[7] J.-Ph. Ansermet, J. Phys.: Condens. Matter 10 (1998) 6027.
[8] S. Zhang, P.M. Levy, J. Appl. Phys. 69 (1991) 4786.
[9] W.P. Pratt Jr. et al., Phys. Rev. Lett. 66 (1991) 3060.
[10] P.A. Schroeder et al., in: R.F.C. Farrow, et al., (Eds.), NATO ASI Series, Magnetism and Structure in Systems of Reduced Dimension, Plenum Press, New York, 1993, p. 129.
[11] P.A. Schroeder et al., Mater. Res. Symp. Proc. 313 (1993) 47.
[12] M.A.M. Gijs et al., Phys. Rev. Lett. 70 (1993) 3343.
[13] M.A.M. Gijs et al., J. Appl. Phys. 75 (1994) 6709.
[14] T. Valet, A. Fert, Phys. Rev. B 48 (1993) 7099.
[15] S.Y. Hsu et al., Phys. Rev. Lett. 78 (1997) 2652.
[16] C. Vouille et al., J. Appl. Phys. 81 (1997) 4573.
[17] P.A. Schroeder et al., J. Magn. Magn. Mater. 177–181 (1998) 1464.
[18] W. Park et al., J. Appl. Phys. 85 (1999) 4542.
[19] A.C. Reilly et al., J. Magn. Magn. Mater. 195 (1999) 269.
[20] I.A. Campbell, A. Fert, in: E.P. Wohlfarth (Ed.), Ferromagnetic Materials, Vol. 3, North-Holland, Amsterdam, 1982, p. 751, Chapter. 9.
[21] I. Mertig et al., J. Magn. Magn. Mater. 151 (1995) 363, and references therein.
[22] S.-F. Lee et al., J. Magn. Magn. Mater. 118 (1993) L1.
[23] J. Barnas, A. Fert, J. Magn. Magn. Mater. 136 (1994) 260.
[24] J. Barnas, A. Fert, Phys. Rev. B 49 (1994) 12835.
[25] S.-F. Zhang, P.M. Levy, Phys. Rev. Lett. 77 (1996) 916.
[26] S.-F. Zhang, P.M. Levy, Phys. Rev. B 57 (1998) 5336.
[27] E.E. Fullerton et al., Phys. Rev. Lett. 68 (1992) 859.
[28] K. Takanashi et al., J. Phys. Soc. Japan 61 (1992) 1169.
[29] A. Kamijo, H. Igarashi, J. Appl. Phys. 72 (1992) 3497.
[30] N.M. Rensing et al., J. Magn. Magn. Mater. 121 (1993) 436.
[31] R. Belien et al., Phys. Rev. B 50 (1994) 9957.
[32] R. Shad et al., Phys. Rev. B 57 (1998) 13692.
[33] W.C. Chiang et al., Phys. Rev. B 58 (1998) 5602.
[34] B. Dieny, Europhys. Lett. 17 (1992) 261.
[35] R.Q. Hood, L.M. Falicov, Phys. Rev. B 46 (1992) 8287.
[36] S.F. Lee et al., Phys. Rev. B 52 (1995) 15426.
[37] S. Steenwyk et al., J. Magn. Magn. Mater. 170 (1997) L1.
[38] W.P. Pratt et al., IEEE Trans. Magn. 33 (1997) 3505.
[39] W.-C. Chiang et al., J. Appl. Phys. 81 (1997) 4570.
[40] L. Piraux et al., Eur. Phys. J. B 4 (1998) 413.
[41] L. Piraux et al., Appl. Phys. Lett. 65 (1994) 2484.
[42] A. Blondel et al., Appl. Phys. Lett. 65 (1994) 3019.
[43] K. Liu et al., Phys. Rev. B 51 (1995) 7381.
[44] S.K.J. Lenczowski et al., J. Appl. Phys. 75 (1994) 5154.
[45] J.E. Wegrowe et al., Helv. Phys. Acta 70 (1997) S5.
[46] M.A.M. Gijs et al., J. Magn. Magn. Mater. 151 (1995) 333.
[47] M.A.M. Gijs et al., Appl. Phys. Lett. 66 (1995) 1839.
[48] T. Ono, T. Shinjo, J. Phys. Soc. Japan 64 (1995) 363.
[49] T. Shinjo, T. Ono, J. Magn. Magn. Mater. 177–181 (1998) 31.
[50] P.M. Levy et al., Phys. Rev. B 52 (1995) 16049.
[51] B. Doudin et al., J Appl. Phys. 79 (1996) 6090.
[52] L. Piraux et al., J. Magn. Magn. Mater. 156 (1996) 317.
[53] L. Piraux et al., J. Magn. Magn. Mater. 159 (1996) L287.
[54] P. Holody et al., Phys. Rev. B 58 (1998) 12230.
[55] S. Dubois et al., Appl. Phys. Lett. 70 (1997) 396.
[56] T. Shinjo, H. Yamamoto, J. Phys. Soc. Japan 59 (1990) 3061.
[57] B. Dieny et al., Phys. Rev. B 43 (1991) 1297.
[58] B. Dieny et al., J. Appl. Phys. 69 (1991) 4774.
[59] Q. Yang et al., Phys. Rev. B51 (1995) 3226.
[60] W.P. Pratt et al., J. Appl. Phys. 79 (1996) 5811.
[61] S.D. Steenwyk et al., J. Appl. Phys. 81 (1997) 4011.
[62] A. Reilly et al., IEEE Trans. Magn. 34 (1998) 939.
[63] P.A. Schroeder et al., J. Appl. Phys. 76 (1994) 6610.
[64] J.A. Borchers et al., submitted for publication.
[65] P. Holody, Ph. D. Thesis, Michigan State University, 1996 (unpublished).
[66] N.J. List et al., Phys. Rev. Lett. 82 (1999) 2796.
[67] J. Bass et al., Mater. Sci. Eng. B 31 (1995) 77.
[68] W.P. Pratt Jr. et al., J. Magn. Magn. Mater. 126 (1993) 406.
[69] J.J. Krebs et al., J. Appl. Phys. 79 (1996) 6084.
[70] M. Johnson, R.H. Silsbee, Phys. Rev. B 35 (1987) 4959.
[71] C. van Son et al., Phys. Rev. Lett. 58 (1987) 2271.
[72] A. Fert, J.-L. Duvail, T. Valet, Phys. Rev. B 52 (1995) 6513.
[73] P.A. Schroeder et al., Mater. Res. Soc. Symp. Proc. 313 (1993) 47.
[74] R.A. de Groot et al., Phys. Rev. Lett. 50 (1983) 2024.
[75] G.L. Bona et al., Solid State Commun. 56 (1985) 391.
[76] J.A. Caballero et al., J. Vac. Sci. Technol. A 16 (1998) 1801.
[77] P. Holody et al., Phys. Rev. B 58 (1998) 12230.
[78] J.M. George et al., Phys. Rev. Lett. 72 (1994) 408.
[79] W.P. Pratt Jr. et al., J. Appl. Phys. 73 (1993) 5326.
[80] L.L. Henry et al., Phys. Rev. B 54 (1996) 12336.
[81] C. Fierz et al., J. Phys.: Condens. Matter 2 (1990) 9701.
[82] A. Vedyayev et al., Phys. Rev. B 55 (1997) 3728.
[83] P. Dauguet et al., Phys. Rev. B 54 (1996) 1083.
[84] B. Dieny et al., J. Appl. Phys. 79 (1996) 6370.
[85] S. Dubois et al., Phys. Rev. B, in press.
[86] A.C. Reilly et al., J. Magn. Magn. Mater., in press.
[87] W. Park et al., J. Appl. Phys., in press.
[88] M. Johnson, Phys. Rev. Lett. 70 (1993) 2142.
[89] Q. Yang et al., Phys. Rev. Lett. 72 (1994) 3274.
[90] S.Y. Hsu et al., Phys. Rev. B 54 (1996) 9027.
[91] L. Piraux et al., J. Magn. Magn. Mater. 159 (1996) L287.
[92] B. Doudin et al., J. Appl. Phys. 79 (1996) 6090.
[93] W. Park et al., unpublished.
[94] D. Baxter et al., J. Appl. Phys. 85 (1999) 4545.
[95] T.R. Werner et al., Phys. Rev. B 26 (1982) 2224.
[96] W. Vavra et al., Appl. Phys. Lett. 66 (1995) 2579.
[97] K.M. Schep et al., Phys. Rev. Lett. 74 (1995) 586.
[98] J. Mathon, Phys. Rev. B 54 (1996) 55.

[99] J. Mathon, Phys. Rev. B 55 (1997) 960.
[100] M.V. Tsoi et al., J. Appl. Phys. 81 (1997) 5530.
[101] W.-C. Chiang et al., Proc. MRS 475 (1997) 451.
[102] S.K. Upadhyay et al, Phys. Rev. Lett. 81 (1998) 3247.
[103] L. Berger, Phys. Rev. B 54 (1996) 9353.
[104] L. Berger, J. Appl. Phys. 81 (1997) 4880.
[105] J.C. Slonczewski, J. Magn. Magn. Mater. 159 (1996) L1.
[106] M.V. Tsoi et al., Phys. Rev. Lett. 80 (1998) 4281.
[107] D.J. Monsma et al., Phys. Rev. Lett. 74 (1995) 5260.
[108] D.J. Monsma et al., Science 281 (1998) 407.
[109] T. Kinno et al., Phys. Rev. B 56 (1997) R4391.
[110] P.N. First et al., J. Appl. Phys. 81 (1997) 553 (Abstract only).
[111] F. Taddei et al., Phys. Rev. Lett., in press.
[112] S. Zhang, P.M. Levy, Phys. Rev. Lett. 81 (1998) 5660.
[113] A. Fert, L. Piraux, J. Magn. Magn. Mater. 200 (1999) 338.
[114] J.E. Wegrowe et al., IEEE Trans. Magn. 34 (1998) 903.